

1 **Ultrastructural changes in colonic epithelial cells in a rat model of inflammatory**
2 **bowel disease**

3
4 **Running title:** Ultrastructural changes in IBD-model rat (40/40 characters)

5
6 Hiroki Bochimoto^{1,2,†,*}, Daisuke Kondoh^{3,†}, Ryuji Nagata^{2,4}, Yo Ishihara⁵, Jumpei
7 Tomiyasu⁶, Kyu-Ho Han², Kenichiro Shimada², Motoki Sasaki³, Nobuo Kitamura³,
8 Michihiro Fukushima²

9
10 ¹Health Care Administration Center, Obihiro University of Agriculture and Veterinary
11 Medicine, Nishi 2-11 Inada-cho, Obihiro 080-8555, Japan

12 ²Department of Life and Food Sciences, Obihiro University of Agriculture and Veterinary
13 Medicine, Nishi 2-11 Inada-cho, Obihiro 080-8555, Japan

14 ³Laboratory of Veterinary Anatomy, Obihiro University of Agriculture and Veterinary
15 Medicine, Nishi 2-11 Inada-cho, Obihiro 080-8555, Japan

16 ⁴The United Graduate School of Agricultural Sciences, Iwate University, 3-18-8 Ueda,
17 Morioka 020-8550, Japan

18 ⁵Asahikawa Medical University, Higashi 2-1-1-1 Midorigaoka, Asahikawa 078-8510,
19 Japan

20 ⁶Laboratory of Theriogenology, Obihiro University of Agriculture and Veterinary
21 Medicine, Nishi 2-11 Inada-cho, Obihiro 080-8555, Japan

22
23 [†]Hiroki Bochimoto and Daisuke Kondoh should be considered joint first author.

25 ***Correspondence**

26 Hiroki Bochimoto, Health Care Administration Center, Obihiro University of Agriculture
27 and Veterinary Medicine, Nishi 2-11 Inada-cho, Obihiro, Hokkaido, Japan.

28 Email: botimoto@obihiro.ac.jp

29

30 **ABSTRACT**

31 Inflammatory bowel disease (IBD) is a global, chronic intractable disease. The functions
32 of drugs and food components have been evaluated in models of IBD induced by 2,4,6-
33 trinitrobenzene sulfonic acid (TNBS). Here, we used transmission (TEM) and osmium-
34 maceration scanning (SEM) electron microscopy to evaluate the ultrastructure of colonic
35 epithelial cells in rat models of IBD induced by TNBS. Histological evaluation revealed
36 that the intestinal crypts in the most regions of the IBD-model colons were deformed and
37 we classified them as having high cell migration rates (HMIG). The remaining regions in
38 the intestinal crypts retained a relatively normal structure and we classified them as
39 having low cell migration rates (LMIG). Osmium-maceration SEM revealed the mucosal
40 fluid flowing in spaces without secretory granules in crypt goblet cells of both HMIG and
41 LMIG regions, indicating the depletion of goblet cell mucin that is found in patients with
42 IBD. The Golgi apparatus in absorptive cells was stacked and curled in both regions.
43 Osmium-maceration SEM showed membrane network structures resembling
44 endoplasmic reticulum that were large and expanded in absorptive cells with HMIG rather
45 than with LMIG regions in IBD-model colons. These findings indicated that endoplasmic
46 reticulum stress is associated with susceptibility to IBD and that the effects of various
47 agents can be evaluated according to endoplasmic reticulum stress revealed by using
48 electron microscopy in models of IBD induced by TNBS. (224/250 words)

49

50 **KEYWORDS**

51 absorptive cells, crypt goblet cells, endoplasmic reticulum stress, Golgi apparatus, mucin
52 secretion

53

54 **RESEARCH HIGHLIGHTS**

55 ✓ Secretory granules are depleted in colonic crypt goblet cells of rat models of IBD.

56 ✓ TNBS induces ER stress-like structures in colonic epithelial cells.

57 ✓ Golgi apparatus is deformed in colonic epithelial cells.

58 (219/250 characters)

59

60 **1. INTRODUCTION**

61 Inflammatory bowel disease (IBD) is a chronic, intractable and costly disease with a
62 prevalence of > 0.3 % in North America, Oceania and most countries in Europe (Ng et
63 al., 2018). Furthermore, the incidence of IBD has increased in Asia, Africa and South
64 America (Ng et al., 2018), indicating a global need for IBD prevention and treatment.
65 Pathological assessment has shown that immune cells migrate into the colonic tissues and
66 that crypt goblet cells are depleted of secretory granules in patients with IBD (Riddle,
67 2004). The mechanism of IBD onset is associated with endoplasmic reticulum (ER) stress
68 of the intestinal epithelial cells (Ma et al., 2017), and it has been suggested that oral
69 administration of substances depressing ER stress dramatically alleviated inflammatory
70 process of IBD induced by dextran sodium sulfate (Cao et al., 2013).

71 Animal models are produced by introducing 2,4,6-trinitrobenzene sulfonic acid
72 (TNBS) into the colon, where it induces colonic lesions like those of human IBD (Talapka
73 et al., 2014; Morampudi et al., 2014). The functions of drugs and food components
74 associated with IBD inhibition have been evaluated in such models (Pfeiffer, Sato, Qiu,
75 Keith, & Evangelista, 1997; Valcheva-Kuzmanova, Kuzmanov, Kuzmanova, & Tzaneva,
76 2018). Although TNBS-induced colonic lesions have mostly been evaluated
77 histologically, more detail ultrastructural evaluation of IBD models is required to
78 understand the mechanism of IBD inhibition. Ultrastructural changes in colonic epithelial
79 cells induced by TNBS have been described (Pfeiffer et al., 1997; Tian, Huang, Tian, Gao,
80 & Chang, 2003; Bou-Fersen, Anim, & Khan, 2008). However, most of these were
81 analyzed by using only transmission electron microscopy (TEM).

82 Osmium-maceration scanning electron microscopy (SEM) allows visualization of
83 three-dimensional ultrastructural architectures after removing soluble protein (Tanaka &

84 Naguro, 1981; Bochimoto et al., 2017; Koga, Bochimoto, Kusumi, Ushiki, & Watanabe,
85 2017). The present study compared colonic epithelial cells in rat models of IBD induced
86 by TNBS and control rats using TEM and osmium-maceration SEM to identified detailed
87 ultrastructural changes.

88

89 **2. MATERIALS AND METHODS**

90 **2.1. Animals**

91 Twelve seven-week-old male Fischer 344 rats (Charles River Laboratories International,
92 Inc., Yokohama, Japan) were used in this study: six were administrated TNBS and six
93 saline. All of these rats were examined by histological and osmium-maceration SEM
94 analyses, and, among these, two rats for each group were also processed for TEM analysis.
95 This study proceeded according to the Regulations on the Management and Operation of
96 Animal Experiments, and the Animal Care and Use Committee of Obihiro University of
97 Agriculture and Veterinary Medicine approved the experimental protocol (Approval
98 number 18-86).

99

100 **2.2. Preparation of rat models of IBD**

101 The rat bowels were emptied by injecting 0.5 mL of 10% glycerin into the anus, then
102 either 0.25 mL of 50% ethanol containing TNBS (120 mg/mL) or sterilized saline was
103 delivered to the colon 45 min later by advancing the tip of a polypropylene catheter
104 (diameter 1.5 mm) to a point 80 mm from the anus. During TNBS treatment, the rats were
105 kept in a head-down position for 1 min under anesthetic condition by using an
106 intraperitoneal injection of pentobarbital (50 mg/kg body weight). Ten days later, the rats
107 were anesthetized by pentobarbital and then euthanized by cervical dislocation. The colon

108 near the site of administration was excised and trimmed into small blocks that were fixed
109 in 10% neutral formalin for histological procedures, or in 0.1 M phosphate buffer (pH
110 7.4) containing 0.5% paraformaldehyde and 0.5% glutaraldehyde for ultrastructural
111 analyses.

112

113 **2.3. Histological procedures**

114 Specimens embedded in paraffin using standard procedures were sliced into 5- μ m-thick
115 sections and stained with hematoxylin-eosin to evaluate tissue injury.

116

117 **2.4. Transmission electron microscopy (TEM)**

118 Colon blocks were post-fixed with 1% OsO₄ for 30 min, dehydrated and then embedded
119 in LR White resin. Ultrathin sections (80 nm thick) were cut using a diamond knife and
120 examined using an HT7700 transmission electron microscope (Hitachi, Tokyo, Japan)
121 without uranyl acetate and lead citrate staining. Semi-thin sections (1 μ m thick) were also
122 cut and stained with toluidine blue to confirm the degree of tissue injury in the specimens.

123

124 **2.5. Osmium-maceration scanning electron microscopy (SEM)**

125 Osmium maceration was applied as described (Bochimoto et al., 2017). Briefly, colon
126 blocks were immersed in 1% OsO₄ for six hours followed by 25% and 50% dimethyl
127 sulfoxide, frozen with a flat aluminum block precooled in liquid nitrogen, and broken into
128 two pieces using a screwdriver and a hammer. The specimens were immersed in 0.1%
129 OsO₄ for 96 h at 20°C, post-fixed in 1% OsO₄, stained with tannic acid and 1% OsO₄,
130 dehydrated and lyophilized in an ES2030 freeze-dryer (Hitachi) with t-butyl alcohol. The
131 specimens were then mounted onto a metal plate, lightly coated with platinum-palladium

132 in an E1010 ion sputter coater (Hitachi) and evaluated using an S4100 scanning electron
133 microscope (Hitachi).

134

135 **3. RESULTS**

136 **3.1. Histological findings**

137 Macroscopically broad inflammation was evident in the colons of the IBD rats (Figure
138 1A). Although the intestinal crypts in most regions of these colons were deformed or
139 absent (Figure 1D), the remaining regions retained the relatively normal structure of the
140 intestinal crypts found in the control colons (Figure 1B, C). The regions with the
141 deformed crypts contained many immune cells and were classified as having high
142 migration rates (HMIG). On the other hand, the number of immune cells in the regions
143 with the relatively normal crypts was comparable to that of controls, and such regions
144 were classified as having low migration rates (LMIG).

145

146 **3.2. Ultrastructural findings in crypt goblet cells**

147 Crypt goblet cells in control colons contained many small secretory granules (Figure 2A,
148 D), whereas most of those in the HMIG and LMIG regions of IBD colons contained a
149 large vacuolar structure (Figure 2B, C). Osmium-maceration SEM revealed that mucosal
150 fluid covering the surface of the epithelium flowed into spaces without secretory granules
151 to form large vacuolar structures in IBD colons (Figure 2E).

152

153 **3.3. Ultrastructural findings of absorptive epithelial cells**

154 Absorptive epithelial cells in control colons contained flat Golgi apparatus in perinuclear
155 regions (Figure 3A, D), whereas those in the HMIG region of IBD colons contained

156 stacked and curled Golgi apparatus (Figure 3C). Some Golgi apparatus in absorptive
157 epithelial cells in the LMIG region were also stacked and curled (Figure 3B, E). Analysis
158 using TEM revealed small vesicular structures in the apical region of epithelial cells.
159 These vesicles were respectively abundant and moderately abundant in the HMIG and
160 LMIG regions of IBD colons (Figure 4B, C), whereas control colons contained only a
161 few vesicles (Figure 4A). Osmium-maceration SEM induces precipitation of soluble
162 proteins revealing cellular membrane compartments where apical cytosol was removed
163 in the absorptive epithelial cells of control colons (Figure 4D). In IBD colons the apical
164 cytosol presented membrane network structures comprising many tubules (Figure 4E, F).
165 The membrane structures were large and expanded in the HMIG region (Figure 4F).

166

167 **4. DISCUSSION**

168 The present study used TEM and osmium-maceration SEM to analyze the colons of rat
169 model of IBD induced by TNBS, and found three types of ultrastructural changes in
170 colonic epithelial cells of the models. Because colons with IBD are pathologically
171 inflamed, the LMIG region of IBD colons did not represent typical IBD lesions. However,
172 ultrastructural changes in colonic epithelial cells of the LMIG and HMIG regions were
173 more or less similar, and thus whether these changes are meaningful as models of IBD
174 should be addressed.

175 The present findings indicated that the depletion of crypt goblet cell mucin occurs
176 in IBD colons like in that of patients with IBD (Riddle, 2004). Although whether large
177 vacuolar structures in IBD colons are fusions or depleted spaces of secretory granules
178 was not evaluated by using only TEM analysis, osmium-maceration SEM significantly
179 revealed that it was the result of depletion of the granules. Because goblet cells in

180 intestinal crypts release mucin in response to endogenous secretagogues associated with
181 some neurotransmitters (Phillips, Phillips, & Neutra, 1984), these cells in the LMIG
182 region could also indirectly receive the inflammatory stimuli via enteric nerves and secrete
183 the granules.

184 The absorptive epithelial cells of IBD colons contained small vesicular structures
185 in the apical region according to TEM analysis. Osmium-maceration SEM revealed that
186 these vesicles were a part of membrane network structures that were defined as ER based
187 on the morphological features. The ER-like structures were larger and expanded in the
188 HMIG region, indicating that ER stress with the expansion is induced by TNBS in colonic
189 epithelial cells, especially in severe inflammatory lesions, of rat models of IBD.
190 Endoplasmic reticulum stress is a critical factor associated with susceptibility to IBD (Ma
191 et al., 2018), and the present ultrastructural findings of epithelial cells seem useful and
192 important in terms of using models of IBD induced by TNBS to evaluate the effects of
193 agents that will be used to treat IBD. The Golgi apparatus was deformed in both the HMIG
194 and LMIG regions of IBD colons. However, the degree of Golgi apparatus deformation
195 was similar between the HMIG and LMIG, and deformed Golgi apparatus is not a general
196 pathology of IBD. Therefore, it is suggested that deformation of Golgi apparatus is not
197 caused by inflammatory responses, and the structural changes seem caused by
198 cytotoxicity of TNBS itself with no relation to IBD.

199 Morphological changes among organelles in epithelial cells induced by TNBS have
200 been described. Pfeiffer et al. (1997) have also identified large amounts of vesicular
201 structures in the apical regions of absorptive epithelial cells induced by TNBS. Bou-
202 Fersen et al. (2008) described deformations of the ER and Golgi apparatus, as well as
203 swollen mitochondria in colons administered with TNBS. Tian et al. (2003) also

204 described that TNBS induces mitochondrial swelling in colonic epithelial cells. The
205 present osmium-maceration SEM analysis revealed that the area mitochondria occupied
206 is lesser in IBD-model colonic epithelial cells (Figure 4D–F), suggesting the possibility
207 that the activity of mitochondria in colonic epithelial cells is associated with inducing
208 IBD. However, osmium-maceration SEM did not identify significant morphological
209 changes of mitochondria (Figure 4D–F), and thus the ultrastructural effects of various
210 agents should be evaluated using various means.

211

212 **5. CONCLUSION**

213 The functions of drugs and food components for treating IBD are considered to be
214 correctly determined from ultrastructural findings of the colons of animal models of IBD.

215 The present study found that some colonic ultrastructural changes induced by TNBS
216 seemed to be associated with inflammatory processes, whereas others seemed to reflect
217 only TNBS cytotoxicity and were not associated with inflammation. These findings
218 indicate that ultrastructural changes in animal models of IBD induced by TNBS can serve
219 as useful indexes, but whether they are significant in the context of IBD should be
220 carefully evaluated.

221

222 **ACKNOWLEDGMENTS**

223 We thank the laboratory staff and colleagues for their helpful suggestions and technical
224 assistance. We are extremely grateful to Ms. Norma Foster for critical reading of the
225 manuscript.

226

227 **AUTHORS' CONTRIBUTIONS**

228 Conceptualization: HB.

229 Investigation: HB, DK, RN, YI, JT, KHH, SS.

230 Supervision: NK, MF.

231 Writing – original draft: HB, DK.

232 Writing – review & editing: HB, DK, RN, YI, JT, KHH, SS, MS, NK, MF.

233

234 **CONFLICTS OF INTEREST**

235 The authors have no conflicts of interest to declare.

236

237 **REFERENCES**

- 238 Bochimoto, H., Matsuno, N., Ishihara, Y., Shonaka, T., Koga, D., Hira, Y., Nishikawa, Y.,
239 Furukawa, H., Watanabe, T. (2017). The ultrastructural characteristics of porcine
240 hepatocytes donated after cardiac death and preserved with warm machine perfusion
241 preservation. *PLoS One*, 12, e0186352.
- 242 Bou-Fersen, A. M., Anim, J. T., Khan, I. (2008). Experimental colitis is associated with
243 ultrastructural changes in inflamed and uninfamed regions of the gastrointestinal tract.
244 *Medical Principles and Practice*, 17, 190–196.
- 245 Cao, S. S., Zimmermann, E. M., Chuang, B. M., Song, B., Nwokoye, A., Wilkinson, J. E.,
246 Eaton, K. A., Kaufman, R. J. (2013). The unfolded protein response and chemical
247 chaperones reduce protein misfolding and colitis in mice. *Gastroenterology*, 144, 989–
248 1000.
- 249 Koga, D., Bochimoto, H., Kusumi, S., Ushiki, T., Watanabe, T. (2017). Changes in the
250 three-dimensional ultrastructure of membranous organelles in male rat pituitary
251 gonadotropes after castration. *Biomedical Research*, 38, 1–18.
- 252 Ma, X., Dai, Z., Sun, K., Zhang, Y., Chen, J., Yang, Y., Tso, P., Wu, G., Wu, Z. (2017).
253 Intestinal epithelial cell endoplasmic reticulum stress and inflammatory bowel disease
254 pathogenesis: An update review. *Frontiers in Immunology*, 8, 1271.
- 255 Morampudi, V., Bhinder, G., Wu, X., Dai, C., Sham, H. P., Vallance, B. A., Jacobson, K.
256 (2014). DNBS/TNBS colitis models: providing insights into inflammatory bowel
257 disease and effects of dietary fat. *Journal of Visualized Experiments*, 27, e51297.
- 258 Ng, S. C., Shi, H. Y., Hamidi, N., Underwood, F. E., Tang, W., Benchimol, E. I.,
259 Panaccione, R., Ghosh, S., Wu, J. C. Y., Chan, F. K. L., Sung, J. J. Y., Kaplan, G. G.
260 (2018). Worldwide incidence and prevalence of inflammatory bowel disease in the

261 21st century: A systematic review of population-based studies. *The Lancet*, 390, 2769–
262 2778.

263 Pfeiffer, C. J., Sato, S., Qiu, B. S., Keith, J. C., Evangelista, S. (1997). Cellular pathology
264 of experimental colitis induced by trinitrobenzenesulphonic acid (TNBS): protective
265 effects of recombinant human interleukin-11. *Inflammopharmacology*, 5, 363–381.

266 Phillips, T. E., Phillips, T. H., Neutra, M. R. (1984). Regulation of intestinal goblet cell
267 secretion. III. Isolated intestinal epithelium. *American Journal of Physiology*, 247,
268 G674–G681.

269 Riddle, R. H. (2004). Pathology of idiopathic inflammatory bowel disease. In R. B. Sartor
270 & W. J. Sandborn (eds.), *Kirsner's Inflammatory Bowel Diseases*, (6th ed., pp 399–
271 424). Saunders, Philadelphia.

272 Talapka, P., Nagy, L. I., Pál, A., Poles, M. Z., Berkó, A., Bagyánszki, M., Puskás, L. G.,
273 Fekete, É., Bódi N. (2014). Alleviated mucosal and neuronal damage in a rat model of
274 Crohn's disease. *World Journal of Gastroenterology*, 20, 16690–16697.

275 Tanaka K., & Naguro T. (1981). High resolution scanning electron microscopy of cell
276 organelles by a new specimen preparation method. *Biomedical Research*, 2, S63–S70.

277 Tian, L., Huang, Y. X., Tian, M., Gao, W., Chang, Q. (2003). Downregulation of
278 electroacupuncture at ST36 on TNF-alpha in rats with ulcerative colitis. *World Journal
279 of Gastroenterology*, 9, 1028–1033.

280 Valcheva-Kuzmanova, S., Kuzmanov, A., Kuzmanova, V., Tzaneva, M. (2018) Aronia
281 melanocarpa fruit juice ameliorates the symptoms of inflammatory bowel disease in
282 TNBS-induced colitis in rats. *Food and Chemical Toxicology*, 113, 33–39.

283

284 **FIGURE LEGENDS**

285 **Figure 1.** Macroscopic and histological features of control and IBD colons.

286 Mucous membranes of colons (**A**) in control (upper) and IBD (lower) rats. IBD and
287 control rats were injected with TNBS or saline at 80 mm from anus. Hematoxylin-eosin
288 stain (**B–D**) of control (**B**) and of low (LMIG; **C**) and high (HMIG; **D**) migration regions
289 of IBD colons. Asterisk and arrowhead in (**D**) indicate deformed intestinal crypts and area
290 without epithelium, respectively. Bars = 10 mm (**A**) and 100 (**B, C**) and 50 (**D**) μm .

291

292 **Figure 2.** Ultrastructural features of crypt goblet cells in control and IBD colons.

293 Transmission electron microscopy (TEM; **A–C**) and osmium-maceration scanning
294 electron microscopy (SEM; **D, E**) findings of control (**A, D**), LMIG (**B, E**) and HMIG
295 (**C**). Abbreviations: sg, secretory granules; v, vacuolar structure. *Lumen (**A–C**). Red
296 highlights, mucous fluid covering epithelial surface; green highlights, secretory granules
297 in (**D, E**). Bars = 2 μm .

298

299 **Figure 3.** Ultrastructural features of perinuclear region of absorption epithelial cells of
300 control and IBD colons.

301 Findings of TEM (**A–C**) and osmium-maceration SEM (**D, E**) of control (**A, D**), LMIG
302 (**B, E**) and HMIG (**C**). Arrowheads (**A–C**) indicate Golgi apparatus. Red and blue
303 highlights (**D, E**) indicate Golgi apparatus and nuclei, respectively. Bars = 1 μm .

304

305 **Figure 4.** Ultrastructural features of apical region of absorption epithelial cells in control
306 and IBD colons.

307 Findings of TEM (**A–C**) and osmium-maceration SEM (**D–F**) of control (**A, D**), LMIG

308 (B, E) and HMIG (C, F). Arrowheads (A–C) indicate small vesicular structures. Red and
309 green highlights (D–F) indicate membrane network structures and mitochondria,
310 respectively. Abbreviations: mv, microvilli; *Space without cytosol (D–F). Bars = 1 μm .
311

Figure S1. Distribution of immune cells and polysaccharide in control and model colons.

Anti-Iba1 (Code 019-19741; Wako Pure Chemical Industries Ltd., Osaka, Japan) immunostain (**A–C**) and toluidine blue stain (**D–F**) to detect macrophages and mast cells, respectively, in control (**A, D**), LMIG (**B, E**) and HMIG (**C, F**). Arrowheads (**A–C**) indicate Iba1-positive macrophages; arrowheads (**D–F**) indicate metachromatic mast cells. Periodic acid-Schiff reaction (**G–I**) and Alcian blue (pH 2.5) reaction (**J–L**) to detect neutral and acidic polysaccharide, respectively. Inserts in (**I, L**) show high magnification of intestinal crypts. Bars = 100 (**A, B, G, H, J, K**), 50 (**C, I, L**), 20 (**D–F**) μm .

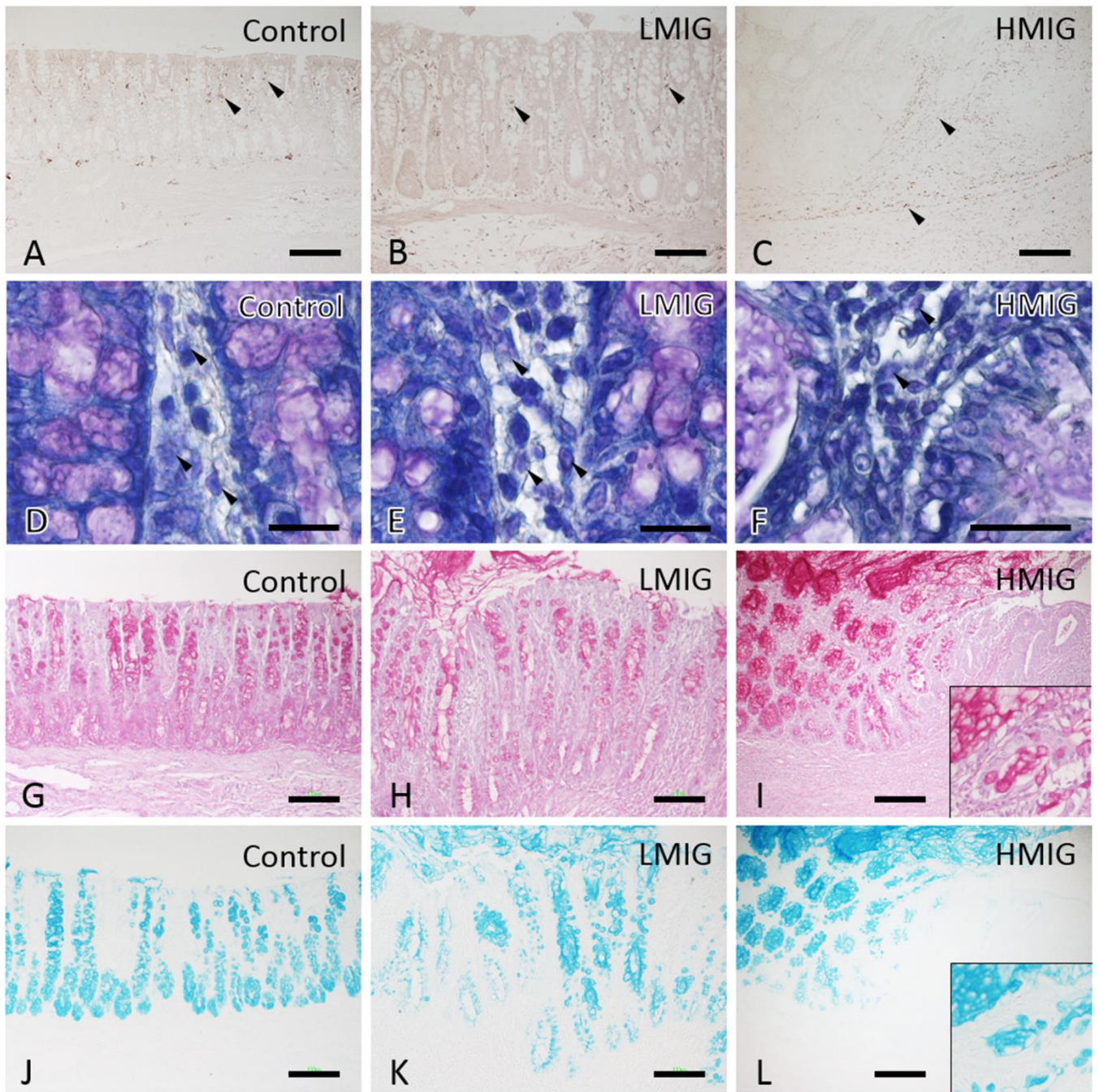
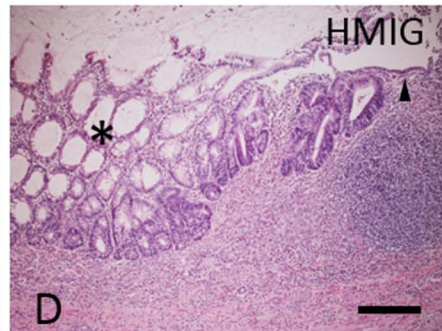
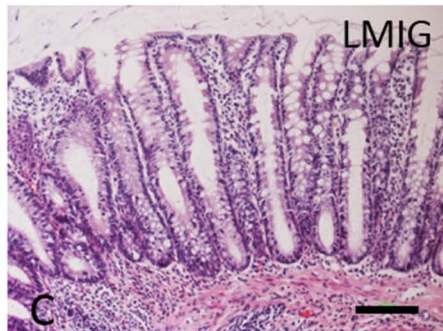
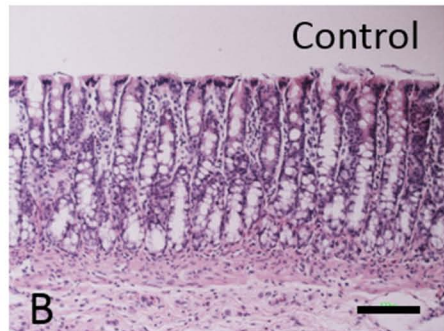
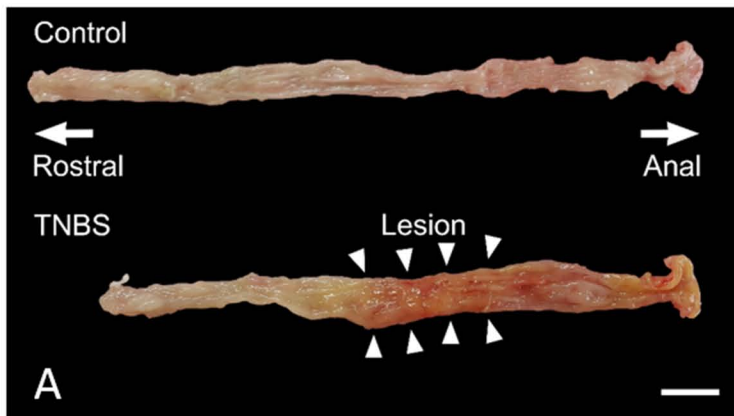
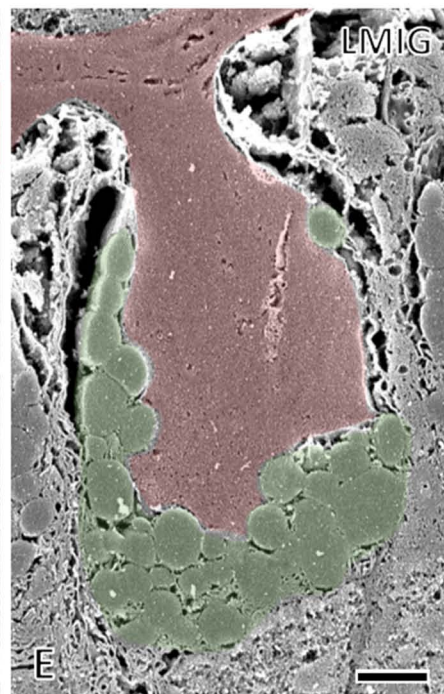
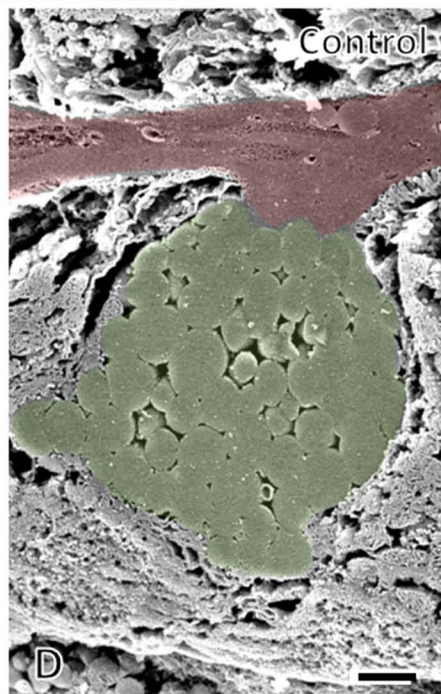
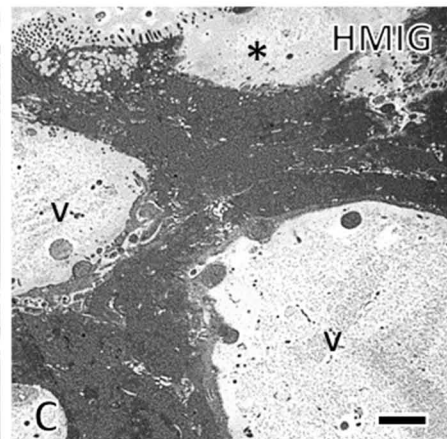
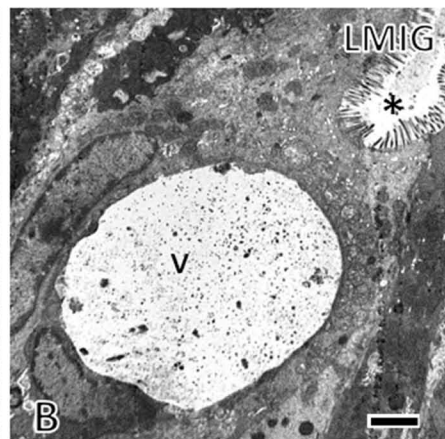
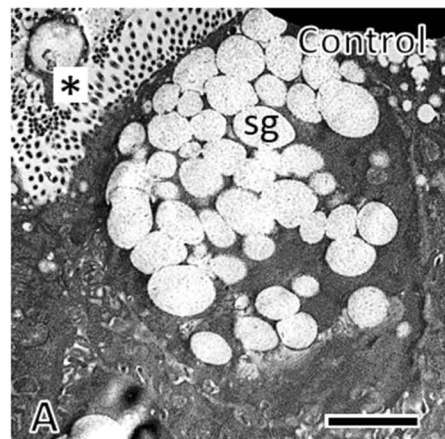
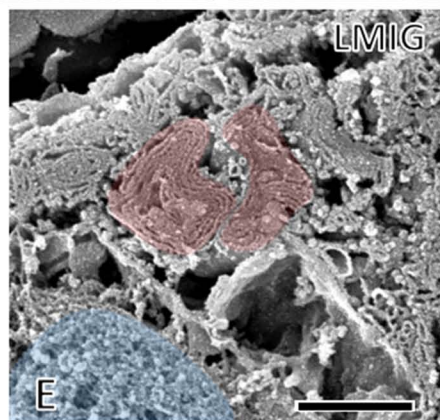
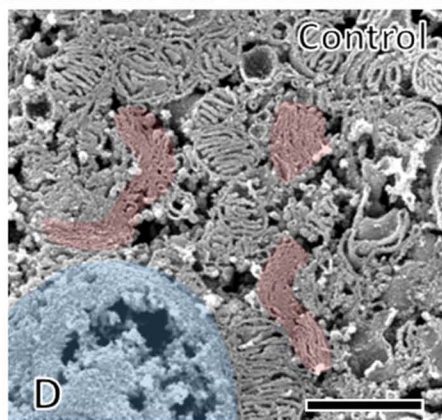
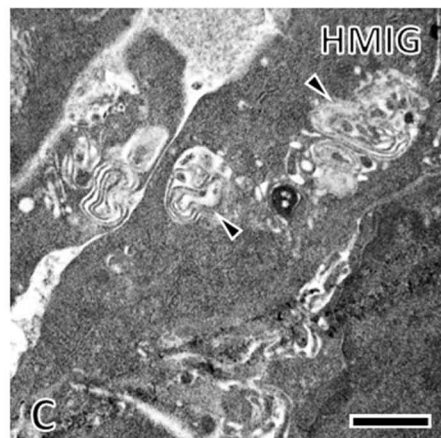
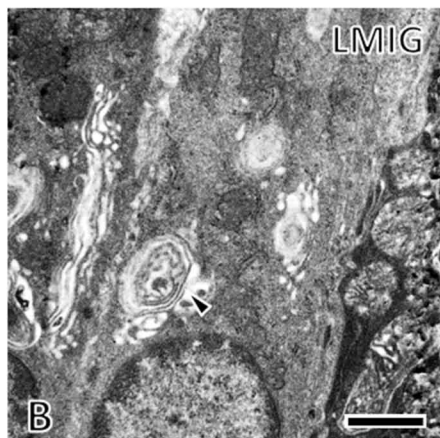
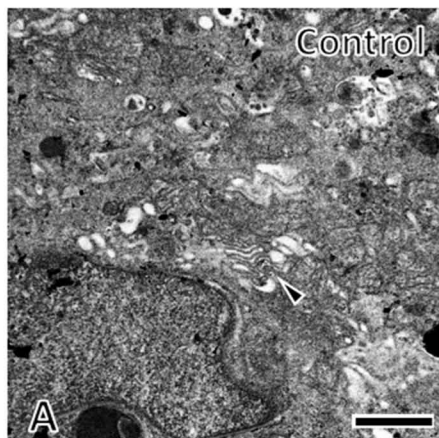
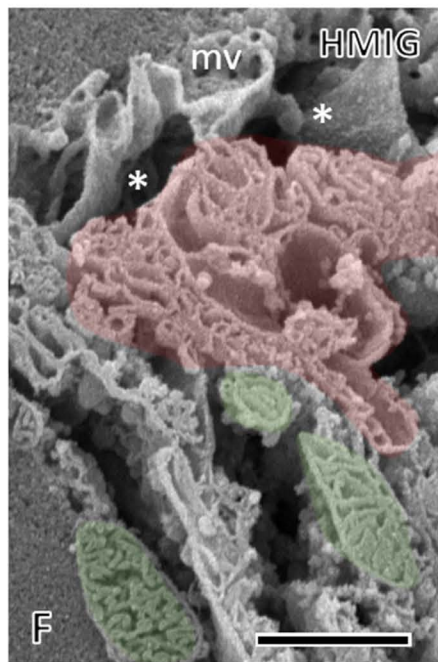
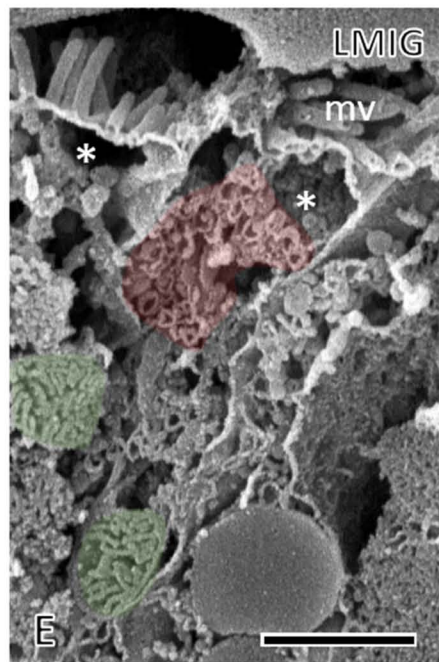
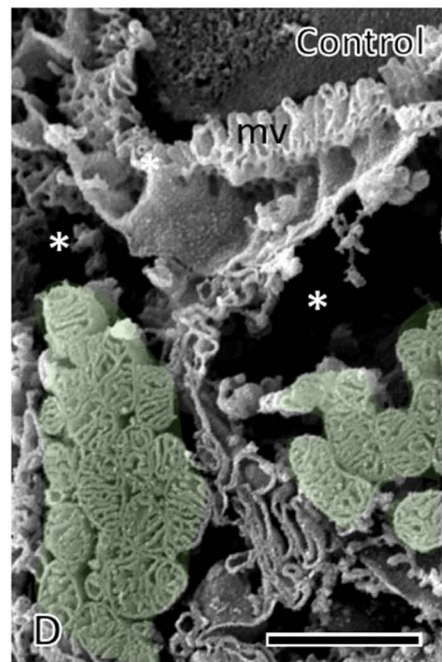
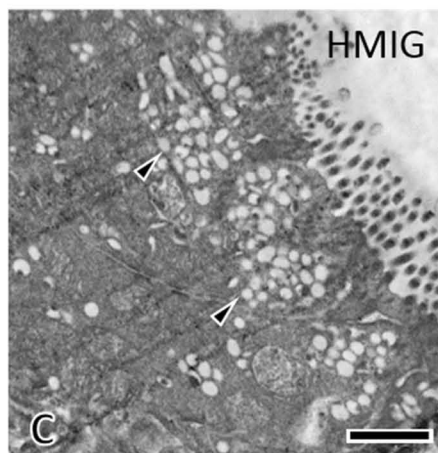
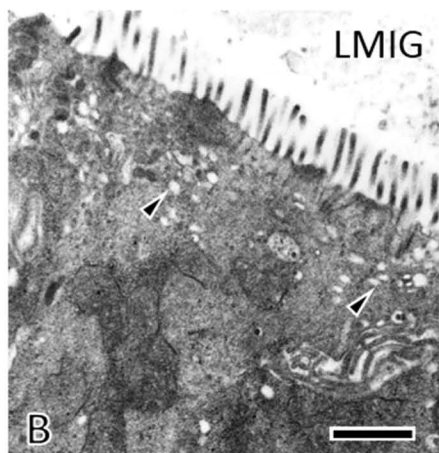
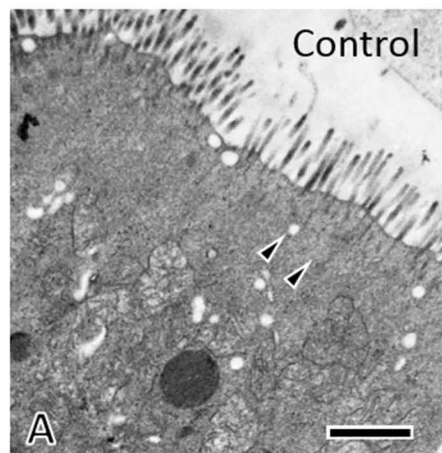


Figure S1

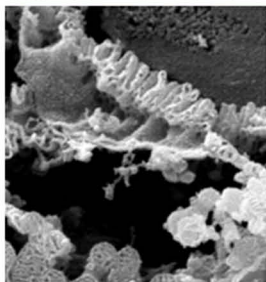
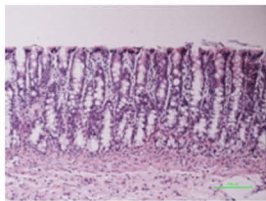
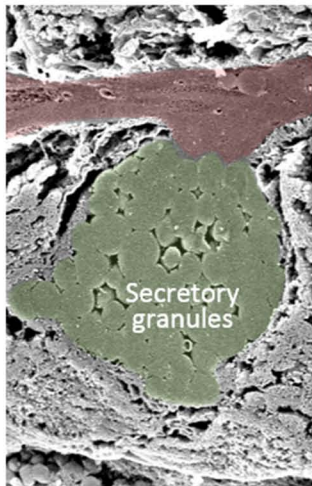








Control rats



Models of IBD induced by TNBS

